In Vivo Imaging of Mammalian Cochlear Blood Flow Using Fluorescence Microendoscopy

*Ashkan Monfared, *Nikolas H. Blevins, *†‡Eunice L. M. Cheung,
†‡§Juergen C. Jung, *Gerald Popelka, and †‡Mark J. Schnitzer

*Department of Otolaryngology–Head and Neck Surgery, †Department of Biological Sciences,
‡Department of Applied Physics, Stanford University, Stanford, California, U.S.A.,
and §Department of Pharmacology, Oxford University, Oxford, U.K.*

Aims: We sought to develop techniques for visualizing cochlear blood flow in live mammalian subjects using fluorescence microendoscopy.

Background: Inner ear microcirculation appears to be intimately involved in cochlear function. Blood velocity measurements suggest that intense sounds can alter cochlear blood flow. Disruption of cochlear blood flow may be a significant cause of hearing impairment, including sudden sensorineural hearing loss. However, inability to image cochlear blood flow in a nondestructive manner has limited investigation of the role of inner ear microcirculation in hearing function. Present techniques for imaging cochlear microcirculation using intravital light microscopy involve extensive perturbations to cochlear structure, precluding application in human patients. The few previous endoscopy studies of the cochlea have suffered from optical resolution insufficient for visualizing cochlear microvasculature. Fluorescence microendoscopy is an emerging minimally invasive imaging modality that provides micron-scale resolution in tissues inaccessible to light microscopy. In this article, we describe the use of fluorescence microendoscopy in live guinea pigs to image capillary blood flow and movements of individual red blood cells within the basal turn of the cochlea.

Methods: We anesthetized eight adult guinea pigs and accessed the inner ear through the mastoid bulla. After intravenous injection of fluorescein dye, we made a limited cochleostomy and introduced a compound doublet gradient refractive index endoscope probe 1 mm in diameter into the inner ear. We then imaged cochlear blood flow within individual vessels in an epifluorescence configuration using one-photon fluorescence microendoscopy.

Results: We observed single red blood cells passing through individual capillaries in several cochlear structures, including the round window membrane, spiral ligament, osseous spiral lamina, and basilar membrane. Blood flow velocities within inner ear capillaries varied widely, with observed speeds reaching up to approximately 500 μm/s.

Conclusion: Fluorescence microendoscopy permits visualization of cochlear microcirculation with micron-scale optical resolution and determination of blood flow velocities through analysis of video sequences. **Key Words:** Capillary—Cochlea—Cochlear blood flow—Fluorescence—Inner ear anatomy—Microcirculation—Microendoscopy.

Otol Neurotol **27:**144–152, 2006.

Cochlear microcirculation appears to be closely linked to hearing function, but the physiologic relationships between the two are poorly understood. Several studies of cochlear blood flow suggest that intense sounds can affect blood velocity, but experimental results as to the magnitude and sign of such effects have varied considerably (1–4). Abnormal blood flow is a putative cause of several forms of sensorineural hearing impairment (5–8), although this subject remains controversial (9). Proposed treatments for hearing loss, such as idiopathic sudden sensorineural hearing loss, that may stem from disruptions in inner ear blood flow have included administration of vasodilators and anticoagulants, which have produced only mixed success (10–13). Further understanding of the relationships between cochlear blood flow and hearing function is important for improving

treatment and diagnosis of deafness that potentially arises from circulatory abnormalities. However, achieving such understanding has been challenging because of the experimental difficulties involved in monitoring cochlear blood flow. Ideally, the study of cochlear circulation should involve in vivo imaging of blood flow with micron-scale resolution within individual vessels of the intact inner ear. Creation of imaging technologies that can provide such data has been stymied by the inner ear's complex geometry, small size, and fragility (14).

To date, most studies of cochlear blood flow in humans and laboratory animals have provided only measurements of bulk flow rates rather than of flow rates within individual vessels. These measurements have generally involved laser Doppler techniques (15–25), which cannot resolve the blood supply to specific cochlear regions, such as the stria vascularis (8) or basilar membrane (1), that are implicated in forms of sensorineural hearing loss. Ultrasound and magnetic resonance imaging are poorer still in this regard and, although unable to resolve cochlear blood flow directly, have revealed clinical correlations between hearing loss and intracranial circulatory disruptions outside the cochlea (7,26–28). Approaches based on injection of either radioactive or labeled microspheres into the bloodstream can allow inferences on the differences in blood flow between cochlear areas (1,18,29). However, such comparisons between cochlear regions rely on histologic samplings of microsphere densities within vessels, precluding real-time imaging of blood flow dynamics. Several intravital microscopy studies of cochlear blood flow in laboratory animals have enabled visualization of flow within individual vessels (30–34), but this approach typically involves extensive surgical resection of temporal bone anatomy, which has prevented application in humans. A few previous studies have explored the use of optical endoscopy within the inner ear for gross anatomic imaging, but poor optical resolution and image quality have to date prevented endoscopic imaging of cochlear microanatomy or microcirculation (35,36).

Recently, our laboratory has developed two forms of minimally invasive in vivo fluorescence imaging, termed one- and two-photon fluorescence microendoscopy (FME) (37–40). These modalities have used endoscope probes composed of compound gradient refractive index (GRIN) microlenses, typically 350 to 1,000 μm in diameter, that provide lateral optical resolution as good as about 0.9 μm (37,38,40). Both forms of FME have enabled in vivo imaging of individual blood cells and neurons within areas of the nervous system too deep to access by conventional microscopy (37–41). In this article, we demonstrate imaging of blood flow dynamics within cochlear capillaries of the live guinea pig using one-photon FME.

MATERIALS AND METHODS

Optical Instrumentation

We used optical instrumentation for one-photon FME that has recently been characterized and documented in detail (Fig. 1A) (37). In brief, we used a custom imaging system constructed on a rail and mounted on a stepper motor-driven X-Y translation stage for imaging studies in small animal subjects. Light from a mercury arc lamp is coupled into a 1.0-mm-diameter illumination delivery fiber. After exiting the fiber, the illumination light passes though a fluorescence excitation filter and is deflected onto the main optical axis by one of several exchangeable dichroic mirrors such that the light overfills the back aperture of a microscope objective (Zeiss Achrostigmat, 10×, numerical aperture (NA) 0.25, Carl Zeiss, Oberkochen, Germany). The objective concentrates illumination light into the endoscope probe. Fluorescence emissions return through the endoscope probe, microscope objective, dichroic mirror, and an emission filter. Fluorescence images can be viewed through the eyepieces of a trinocular or projected onto a camera. There are two mechanisms for focusing the image, implemented through a pair of modular focus units that hold the microscope objective and endoscope probe. One unit adjusts the position of the endoscope probe within the animal subject. The second unit adjusts the position of the microscope objective relative to the endoscope probe, so that the image focus within tissue can be altered without any mechanical movements within the subject. For further details on construction of the optical instrumentation, the reader should consult Jung et al. (37).
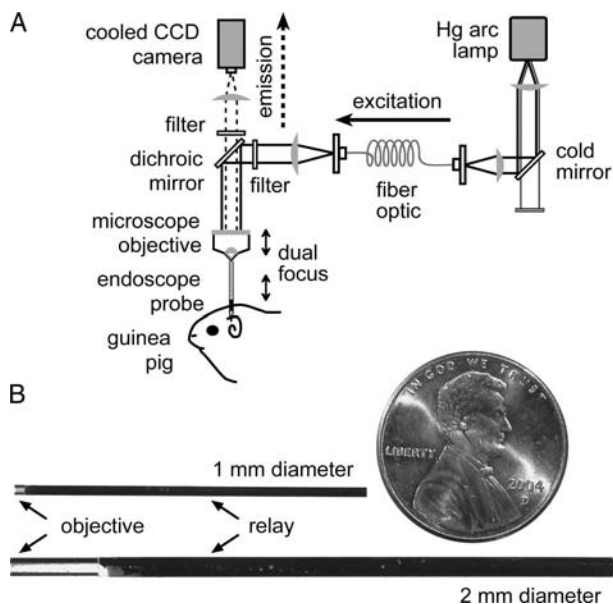

FIG. 1. Optical instrumentation for FME in the guinea pig cochlea. (*A*) Schematic of the imaging instrumentation. Fluorescence excitation light from a mercury arc lamp couples into an illumination delivery fiber, passes through a fluorescence excitation filter, and reflects into a conventional microscope objective via a dichroic mirror. The objective focuses this excitation light onto the back face of the endoscope probe, which delivers the light to the guinea pig cochlea. Fluorescence emission photons return through the endoscope probe, dichroic mirror, and an emission filter, and the fluorescence image can be viewed by eye or projected onto a camera, such as a cooled charge-coupled device camera. (*B*) Photograph of two GRIN doublet endoscope probes, 1.0 and 2.0 mm in diameter, positioned next to a Lincoln penny for size comparison. The probes are oriented with the GRIN objective to the left. The GRIN relay lenses each exhibit a dark coating.

Endoscope Probes

Our compound doublet endoscope probes comprise a GRIN objective and a GRIN relay lens (37) (Fig. 1B). Unlike conventional lenses, which rely on curved surfaces to refract light, such cylindrically symmetric GRIN lenses guide light using a radially varying refractive index profile that arises from spatially inhomogeneous doping with an ion such as silver, thallium, or lithium (42,43). Because GRIN lenses are not ground to shape, they can be economically fabricated in tiny sizes. GRIN objective lenses can exhibit an NA as high as 0.5 to 0.6, facilitating optical imaging with micron-scale resolution (37–40). The main purposes of the GRIN relay, which typically exhibits an NA of approximately 0.08 to 0.2, are to provide the length necessary to reach deep tissues and to project a real image of the specimen plane that can be viewed with the microscope objective.

For the studies described here, we used endoscope probes that were either 1.0 or 2.0 mm in diameter, with a 1,040 μm working distance (WD) in water between the tip of the GRIN objective lens and the focal plane within the specimen. The majority of images acquired in the cochlea, including all those shown in the figure panels, were captured using 1.0-mm-diameter endoscope probes. After some initial exploration in the use of FME within the cochlea, we chose to use endoscope probes with objectives of a lower range of NA values (0.11 and 0.38) than in our previous work (37). This choice comes at the cost of slightly diminished optical resolution. However, the depth of field varies inversely with the square of the NA (44), and we found that the longer depths of field were useful for keeping the entire exposed basal turn of the cochlea in view while navigating in the inner ear with the endoscope probe.

We measured the lateral optical resolution of each endoscope probe by imaging a nanofabricated Siemens star pattern on a Marine Biological Laboratory/National Nanofabrication Facility transmittance test slide (37,45). The Siemens star is a circular pattern in which there are 36 pairs of alternating transparent and opaque wedges. The diameter in the image where contrast between adjacent wedges vanishes provides an estimate of lateral optical resolution according to the Sparrow criterion of zero contrast (37,44). The standard error (SE) in diameter measurements led to the SE in lateral resolution. In this way, we determined the lateral resolution of the 0.11-NA probe to be 3.26 $\pm$ 0.05 μm (mean $\pm$ SE) and that of the 0.38 NA probe to be 1.29 $\pm$ 0.06 μm. The latter measurement is slightly poorer than a previous measurement of the lateral optical resolution limit (0.92 $\pm$ 0.15 μm) of another endoscope probe with the same nominal optical characteristics (0.38 NA, 1,040 μm WD).

To estimate the field of view (FOV) diameter of an endoscope probe, we translated an object in the specimen plane across the extent of the image field in both the X and Y lateral dimensions using the calibrated translation stage on which the microscope is built (Danaher Corp., Salem, NH, U.S.A.). We found that the endoscope probe of 0.11 NA and 1,040 μm WD had a FOV diameter of 943 μm and that the endoscope probe of 0.38 NA and 1040 μm WD had a FOV diameter of 280 μm.

Animals

We used eight female adult albino Hartley guinea pigs (285–510 g) for this study. The Stanford Administrative Panel on Laboratory Animal Care approved all animal procedures.

Surgery

We anesthetized guinea pigs using intraperitoneal injections of ketamine (50 mg/kg) (Vedco, St. Joseph, MO, U.S.A.), xylazine (10 mg/kg) (Vedco), and urethane (1,000 mg/kg) (Sigma-Aldrich, St. Louis, MO, U.S.A.), along with subcutaneous injection of atropine (0.05 mg/kg) (Vedco). After receiving injections, animals sat on a thermal plate. During surgery, we infiltrated a local anesthetic, 1% lidocaine with 1:100,000 epinephrine (Abbott Laboratories, Abbott Park, IL, U.S.A.), into the surgical field.

We accessed the cochlea via a dorsal approach through the mastoid bulla (46), allowing direct exposure of the round window and basal turn of the cochlea. Through a postauricular incision, we opened the dorsal surface of the mastoid bulla with an otologic drill. We identified anatomic landmarks, such as the tympanic membrane annulus, facial nerve, semicircular canals, and external auditory canal wall (Fig. 2). In our initial studies, such structures were resected to provide the endoscope probe perpendicular access to the round window membrane. In later studies, we preserved the tympanic membrane annulus, external auditory canal, and vestibule but sacrificed the facial nerve, ossicles, and lateral semicircular canal to provide sufficient exposure of the round window.

We tested three anatomic placements of the endoscope probe for performing FME in the inner ear. First, we placed the endoscope probe at the round window without transgressing its membrane. This allowed imaging of the vasculature of the round window membrane itself as well as of the most proximal portion of the osseous spiral lamina and basilar membrane. Second, we resected the round window membrane with a sharp pick and introduced the endoscope probe into the scala tympani. This provided additional ability to image the osseous spiral lamina, spiral ligament, and basilar membrane. However, the trajectory of the endoscope probe remained somewhat tangential to the osseous spiral lamina. To address this problem, we used a third method in which we performed a cochleostomy in continuity with the round window using a diamond burr. We resected the antimodiolar wall of the scala tympani to the level of the osseous
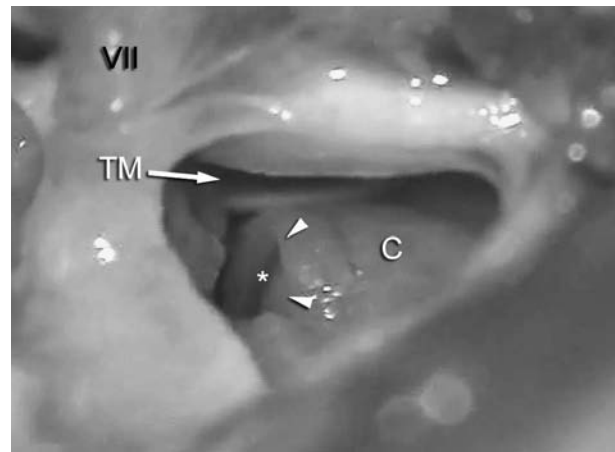

FIG. 2. Surgical view of the right guinea pig cochlea. The cochlea (C) and round window (*arrowheads*) can be clearly seen through the surgical microscope. A dorsal approach through the posterior bulla was used. The basilar membrane (*) is visible through the semitransparent round window membrane. Anatomic limits of this approach include the tympanic membrane (TM) and ossicles on the anterior side. The vestibular system, which is further posterior, is left intact. The facial nerve (VII) is visible as it exits the skull dorsal and posterior to the external auditory canal. We used a dorsal surgical approach of this type to expose the basal turn of the cochlea for subsequent FME.

spiral lamina, keeping the basilar membrane intact. This provided a perpendicular view of the basilar membrane after insertion of the endoscope probe through the cochleostomy.

In all procedures, we used artificial perilymph (145 mmol/L NaCl, 2.7 mmol/L KCl, 2.0 mmol/L MgSO$_4$, 1.2 mmol/L CaCl$_2$, 5.0 mmol/L HEPES buffer, pH 7.4 [Sigma-Aldrich]) for irrigation after creation of the cochleostomy. Animals were euthanized by intraperitoneal injection of Nembutal (Abbott Laboratories) at the conclusion of FME.

Imaging and Video Analysis

Before imaging blood flow by FME, we generally obtained microendoscopic images of the anatomic structures (such as Figs. 3A and 4A) within the image field under bright-field illumination, which was routed from a halogen bulb by fiber optic goosenecks to illuminate the ear at the side of the endoscope probe. To initiate FME, we injected 0.2 ml of fluorescein dye (55 mg/ml) (Sigma-Aldrich) into the femoral vein. After waiting 5 to 10 minutes, we acquired fluorescence video sequences of cochlear blood flow, which were captured using an excitation filter HQ470/40 (Chroma, Rockingham, VT, U.S.A.), a dichroic mirror Q515LP (Chroma), an emission filter OG630 (Zeiss), and a cooled charge-coupled device camera (CoolSnap HQ; Roper, Tucson, AZ, U.S.A.) controlled by commercial imaging software (IPLab; Scanalytics, Inc., Fairfax, VA, U.S.A.).

To estimate the speed of red cell blood flow from digital video records, we traced the movement of individual red blood cells within capillaries providing flow either toward or away from the basilar membrane and calculated the distance traveled between movie frames. Positions were tracked in consecutive video frames (ImageJ; National Institutes of Health, Bethesda, MD, U.S.A.), and speeds were calculated by multiplying the video frame rate by the straight-line displacements of positions in two consecutive frames (Manual Tracking Plug-in, ImageJ). Results from multiple video frames and multiple red blood cells traveling within a single capillary were averaged to yield an estimate of the average blood cell speed within that vessel.

We estimated the diameter of each capillary studied by plotting the vessel's cross-sectional fluorescence intensity profile and measuring the full width above the background fluorescence level (ImageJ). We expect that this procedure may yield overestimates of blood vessel diameters for vessels that were slightly out of focus but may also yield underestimates if the intensity of fluorescence signals from the edge of the cross-sectional vessel profile is below the background fluorescence intensity.

RESULTS

Endoscope Selection

We tested several endoscope probe designs for their ability to visualize cochlear anatomy and blood flow in structures such as the round window, osseous spiral lamina, stria vascularis, and basilar membrane. We sought an optical depth of field sufficient to maintain an entire quarter turn of the cochlea in focus within a single view, because this provided us with the ability to navigate within the cochlea under endoscopic guidance. We found that probes with approximately 1,000 μm or more of optical WD in water from the tip of the endoscope probe to the specimen plane were well suited for imaging the entire exposed basal turn of the cochlea. It was difficult to position endoscope probes with shorter depths of field, because surrounding anatomic landmarks were often out of focus. For this reason, we used a 1.0-mm-diameter, 1,040 μm WD endoscope probe with 0.11 NA and a 943-μm-diameter FOV. The lateral resolution afforded by this endoscope probe was 3.26 ± 0.05 μm (mean ± SE), as determined through quantitative analysis of the image of a nanofabricated Siemens star resolution test pattern (as described above under Materials and Methods) (37,45). For higher resolution imaging of
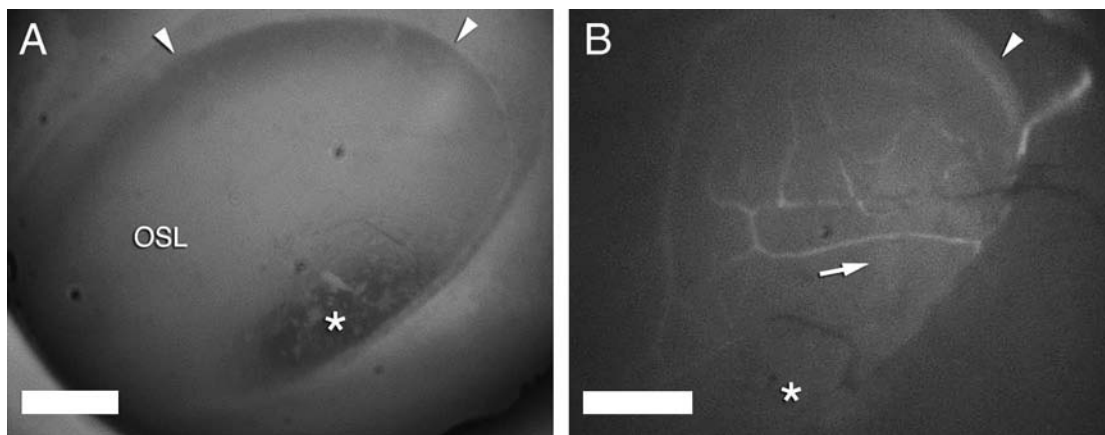

FIG. 3. Images of the guinea pig round window acquired in vivo using microendoscopy. (*A*) View of the right round window obtained using a GRIN microendoscope probe (1 mm diameter, 1,040 μm WD in water, 0.11 NA, 943 μm FOV) under bright-field illumination before intravascular administration of fluorescein. We used a dorsal surgical approach, leaving the round window membrane intact. The osseous spiral lamina (OSL) as well as the location of the basilar membrane (dark streak at *arrowheads*) can be seen through the semitransparent round window membrane. The lumen of the scala tympani's first turn can be seen as a shadow at the periphery of the round window. (*B*) Image acquired by FME of the round window membrane vasculature after administration of fluorescein. The anatomic orientation and endoscope probe were the same as in *A*, with the *arrowhead* pointing to the basilar membrane. The direction of red blood cell flow (*arrow*) was readily apparent on video sequences. The lumen of the first turn of the scala tympani (*) is again visible as a shadow at the periphery of the round window. Scale bars = 200 μm.
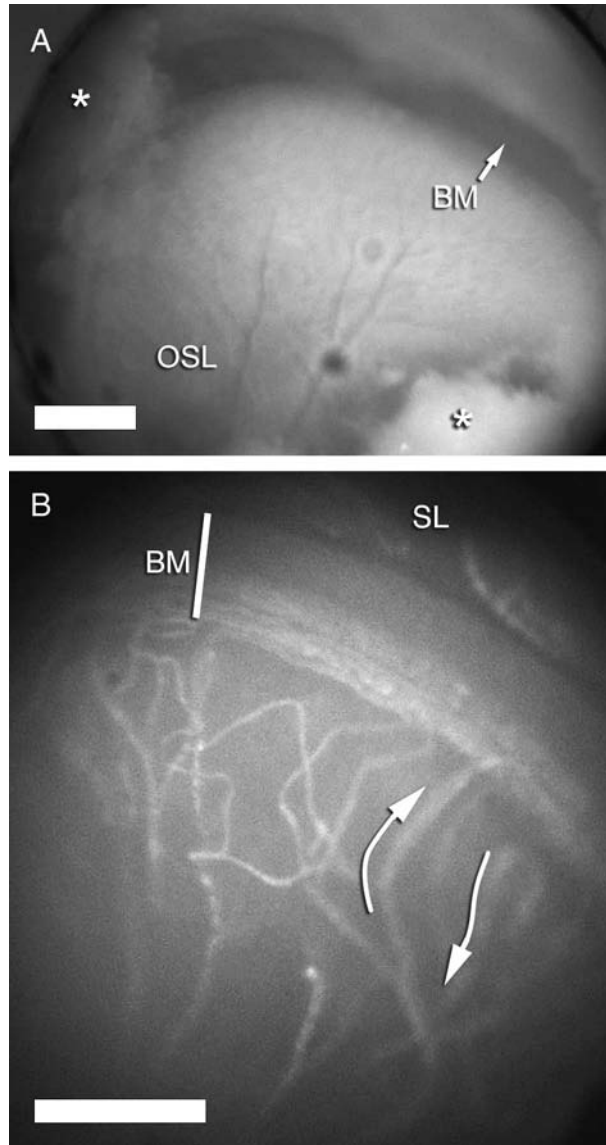
FIG. 5. Red blood cells and capillaries within the osseous spiral lamina imaged in vivo using FME. An image of capillaries and red blood cells (*arrowheads*) within the osseous spiral lamina vasculature, acquired by FME in an anesthetized guinea pig using a 1.0-mm-diameter endoscope probe of 0.38 NA, 280 μm FOV, and 1,040 μm WD. The corresponding video sequence shows the red blood cells progressing single file through the capillaries. Scale bar = 50 μm.

FIG. 4. Images of the osseous spiral lamina and basilar membrane acquired in vivo using microendoscopy. (*A*) Image of the right osseous spiral lamina (OSL) and basilar membrane (BM) in an anesthetized guinea pig, acquired by microendoscopy under bright-field illumination after removing the round window membrane. Some of the basilar membrane remained at the periphery (*), and the vasculature of the osseous spiral lamina can be seen as dark radially oriented lines on the bone. (*B*) Image acquired by FME of the vasculature of the basal turn of the right scala tympani in the same anesthetized guinea pig as in *A*. Vessels of the peripheral osseous spiral lamina and basilar membrane are brightly labeled after fluorescein administration. By tracking the flow of red blood cells, which appear in video sequences as dark entities moving within the bright plasma, we identified blood vessels with flow toward or away from the basilar membrane (*arrows*). Although fewer in number, several vessels within the spiral ligament (SL) are also visible. The images in both panels were acquired with a 1.0-mm-diameter endoscope probe with 0.11 NA, 1,040 μm WD in water, 943 μm FOV. Scale bars = 200 μm.
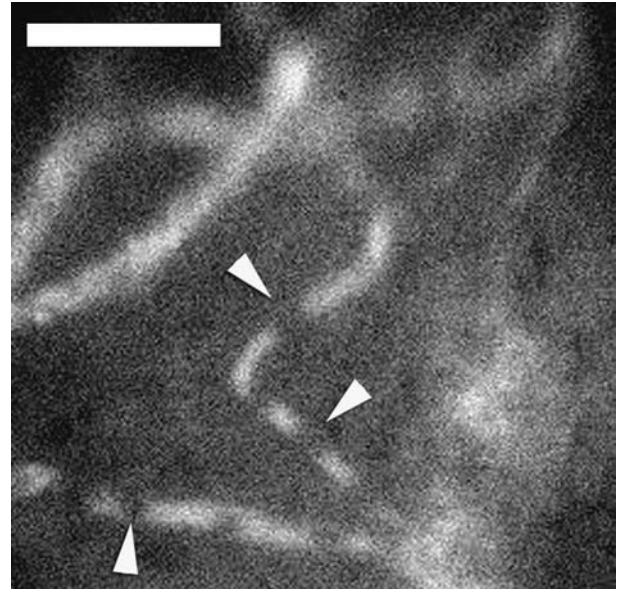
individual red blood cell flow in capillaries, we used a 1.0-mm-diameter endoscope probe with a 1,040 μm WD, 0.38 NA, and 280-μm-diameter FOV, for which the lateral resolution was 1.29 ± 0.06 μm.

Cochlear Blood Flow

We used intravascular administration of fluorescein dye, which labels the blood plasma brightly, to investigate cochlear circulatory dynamics. Under fluorescence imaging, the red blood cells appear dark by comparison with the plasma, allowing measurement of red blood cell speeds (30,32,37,40,47). We were able to observe blood flow in several regions of the cochlea, including the round window membrane, osseous spiral lamina, spiral ligament, and basilar membrane.

We first inserted the endoscope through the surgical opening in the dorsal bulla and focused on the round window membrane. The osseous spiral lamina and basilar membrane were visible through the round window membrane (Fig. 3A). After injection of fluorescein, we could see capillaries on the round window membrane and could determine the direction of the blood flow (Fig. 3B).

After removing the round window membrane and creating a 2-mm-diameter cochleostomy, we obtained a clearer view of the osseous spiral lamina and the basilar membrane (Fig. 4A). We observed blood flow on the osseous spiral lamina, in the spiral ligament, and in the two vessels within the basilar membrane running parallel to the rows of hair cells (Fig. 4B) (5). The

motions of single red blood cells (approximately 8 μm in diameter) were readily apparent on video sequences, as demonstrated previously using FME in other areas of the nervous system (37,40). These cell movements make visual identification of the red blood cells much easier in movies than in still frames, in which cues about directional flow are lacking.

We tested our ability to measure red blood cell velocities by analysis of FME video records and determined the direction and speed of blood cell flow to and from the basilar membrane through the vessels of the osseous spiral lamina (Fig. 5). The speed of erythrocyte flow in the capillaries varied considerably between different cochlear areas, as previously observed by intravital microscopy (31) and as estimated from histologic counts of injected microspheres (29). We estimated the speed of blood flow in several capillaries with apparent cross-sectional diameters ranging from approximately 13 to 24 μm in the osseous spiral lamina of the basal turn. Flow speeds within four capillaries in one FOV of a single animal ranged from approximately 211 to 500 μm/s. In the same set of images, the blood flow in a single approximately 9-μm-diameter vessel in the stria vascularis was slower, ranging from approximately 57 to 88 μm/s, which is consistent with a previous observation by intravital microscopy that flow speeds in the stria vascularis are slow, typically between 30 and 100 μm/s (31). In the round window of another animal, our estimates of blood flow speeds varied from approximately 43 to 271 μm/s in five capillaries with apparent cross-sectional diameters ranging from approximately 10 to 24 μm. These estimates of blood cell speeds are based on a limited number of observations but demonstrate the capability to make such measurements in vivo by using FME.

By directing the endoscope probe more in parallel with the osseous spiral lamina, we were able to examine the curvature of the scala tympani (Fig. 6). We could clearly see the lumen of the scala tympani and the vasculature of the spiral ligament on the antimodiolar wall. However, visualization of red blood cells was sufficiently poor to prevent reliable quantitation of flow speeds in this region.
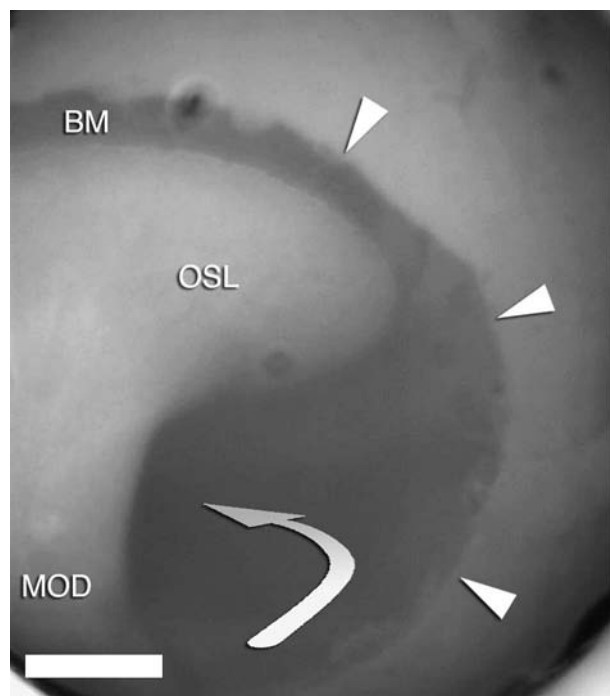

FIG. 6. Imaging the basal turn of the scala tympani by in vivo microendoscopy. The curvature of the lumen of the scala tympani (*arrow*) around the central modiolus (MOD) is visible in this bright field microendoscopic image from the right cochlea of an anesthetized guinea pig and was particularly apparent while varying the image focus. The osseous spiral lamina (OSL) and basilar membrane (BM) are on the apical side of the scala tympani. On switching to fluorescence imaging by FME, blood flow was visible within numerous small vessels in the spiral ligament along the antimodiolar wall of the scala tympani and along the modiolus. For acquisition of this image, the endoscope probe (1.0 mm diameter, 1,040 μm WD, 0.11 NA, 943 μm FOV) was positioned just outside the cochleostomy, with the bony margins indicated by *arrowheads*. Scale bar = 200 μm.

DISCUSSION

There is an unmet need for an inner ear imaging technique that can provide anatomic and physiologic information in live subjects in a relatively nondestructive manner. Such a tool might shed light on fundamental issues concerning hearing function and loss, enable clinically significant diagnostics, and guide future surgical efforts to restore hearing function by micromanipulation. The results of the current study suggest that the use of FME deserves exploration for such applications. This view is supported by a number of previous reports that suggest the clinical potential for cochlear microendoscopy using imaging of scattered light (35,36,48).

In one report, flexible fiberoptic endoscopes (0.35–0.89 mm) were used to evaluate cochleae of patients undergoing repeat cochlear implantation (36). The authors reported that endoscopes were useful in identifying anatomic obstructions of the cochlear scalae that were not always apparent during preoperative imaging studies (36). In another study, endoscopes were used to guide laser recanalization of a cadaveric model of ossified cochlea (35). However, in none of these previous endoscopy applications have the images produced by scattered light been of sufficient contrast and resolution to allow visualization of cochlear microcirculation. Thus, to date, nearly all studies of cochlear blood flow have involved measurements of bulk flow speeds using laser Doppler techniques.

Laser Doppler flowmetry allows determination of blood flow speeds based on the Doppler frequency shift of a reflected laser beam. Placement of the Doppler probe outside the bony otic capsule allows preservation of the cochlea. However, with this experimental configuration, bone blood flow within superficial vessels of the capsule also contributes to the Doppler signal (22). Thus,

there is the potential for inaccuracy, especially because the otic capsule and its surrounding mucosal vasculature are supplied by arteries other than the cochlea (5,49). Moreover, vessels closest to the probe contribute a disproportionately greater signal than more distant vasculature, so the small blood supply to the organ of Corti and to other sensitive neural elements might be obscured by the larger and much closer vessels in the lateral cochlear wall (5,29). Through comparisons with measurements of cochlear blood flow using microsphere-based techniques, the contribution to the laser Doppler signal from blood flow in the otic capsule has been estimated to be 30 to 40% of the total Doppler signal in rats (24). This contribution from bone flood flow is expected to be higher in the thicker walled human cochlea (5). The optical transmission coefficient through the human promontory bone was estimated in one study to be only approximately 1 to 2% for red light of 632-nm wavelength, as compared with values measured in rats and guinea pigs of approximately 15% and approximately 6%, respectively (50). Another study found considerably higher transmission coefficients through the human promontory (49). Nonetheless, Doppler flowmetry has been applied clinically (15,17,25,51). However, the inability of Doppler methods to provide data on flow speeds within specific areas of the cochlea is a major limitation that intravital optical imaging is well suited to address.

Intravital fluorescence microscopy is an optical imaging method that can provide detailed information on blood flow within single cochlear vessels. The technique relies on a long-WD microscope objective to view red blood cells in the cochlea and has been used to determine blood flow speeds within cochlear regions that are visible through a window in the otic capsule (2,3,30–34). However, sacrifice of surrounding structures has been required for placement of the microscope objective sufficiently close to the cochlea to obtain images. Thus, intravital microscopy appears to be best suited for use in animal subjects with easily accessible cochleae, such as the guinea pig, and to our knowledge has not been applied in a clinical setting. However, an optical imaging approach that affords resolution similar to that of microscopy but that does not require sacrificing surrounding structures might hold significant potential for both clinical and research applications. FME appears to be just such an approach. Moreover, we have shown that by inserting an endoscope probe within the cochlea, rather than opening a window in the otic capsule as is done in intravital microscopy studies (32), FME can provide direct views of blood flow in cochlear areas such as the round window and basilar membrane that are not visible through an otic capsule window.

Such use of the endoscope probe within the cochlea has allowed us to estimate red blood cell speeds within the basilar membrane. Unlike Doppler flowmetry, microendoscopy offers the ability to image cochlear microanatomy and blood flow concurrently and does not confound cochlear blood flow with more superficial circulation. Moreover, unlike cochlear imaging by intravital microscopy

(31), FME does not require extensive resection of surrounding anatomy such as middle ear structures. One current limitation to our methodologies concerns the mechanical rigidity of the endoscope probe. The probe cannot bend within the geometric constraints imposed by the cochlear turns. The use of angled endoscope probes might partly alleviate this issue by providing an assortment of viewing angles but would still not allow the probe to be inserted through multiple cochlear turns.

We hope that in the future FME might be used while maintaining inner ear function. A significant limitation is the need for a cochleostomy to introduce the endoscope probe. In the current study, we made no effort to preserve hearing in our experimental animals or to quantify the anatomic and physiologic sequelae of our intervention. We seek to refine the techniques presented here to minimize the cochleostomy diameter, to avoid direct contact of the probe with the basilar membrane or osseous spiral lamina, and then to assess the affect of FME on hearing. Many delicate features of the cochlea, such as the cochlea's sharp frequency tuning and high sensitivity, quickly disappear when the inner ear is opened (14). Nevertheless, investigators have been able to access the guinea pig cochlea at both basal and apical ends without substantial loss of hearing (52–57). Otologic surgeons routinely open the inner ear while preserving hearing during stapedectomy (58–60), and it has also been demonstrated that cochlear implantation can be performed while maintaining useful acoustic function of the implanted cochlea (61,62). Such findings make us think that it may be possible to perform cochlear FME while preserving hearing function.

CONCLUSION

We have visualized blood flow using one-photon FME in several regions of the cochlea, including within individual vessels in the basilar membrane, where transient vascular occlusions may affect the function and viability of the organ of Corti. We have also demonstrated measurements of capillary blood flow speeds through video analysis. Such capability to assess inner ear microcirculation should promote improved diagnostic capability and therapeutic intervention. We anticipate that with further refinement FME may serve both clinical and basic science applications. For example, FME might support work on the design and placement of hearing prostheses (62,63) as well as on microrobotic surgery (64–66), gene therapy (67), and drug delivery within the inner ear (68,69). Moreover, the ability to image cochlear compartments with micron-scale resolution seems likely to benefit basic research on cochlear function.

REFERENCES

1. Prazma J, Rodgers GK, Pillsbury HC. Cochlear blood flow: effect of noise. *Arch Otolaryngol* 1983;109:611–5.

2. Quirk WS, Avinash G, Nuttall AL, et al. The influence of loud sound on red blood cell velocity and blood vessel diameter in the cochlea. *Hear Res* 1992;63:102–7.

3. Quirk WS, Shapiro BD, Miller JM, et al. Noise-induced changes in red blood cell velocity in lateral wall vessels of the rat cochlea. *Hear Res* 1991;52:217–23.

4. Attanasio G, Buongiorno G, Piccoli F, et al. Laser Doppler measurement of cochlear blood flow changes during conditioning noise exposure. *Acta Otolaryngol* 2001;121:465–9.

5. Nakashima T, Naganawa S, Sone M, et al. Disorders of cochlear blood flow. *Brain Res Brain Res Rev* 2003;43:17–28.

6. Seidman MD, Quirk WS, Shirwany NA. Mechanisms of alterations in the microcirculation of the cochlea. *Ann N Y Acad Sci* 1999;884:226–32.

7. De Felice C, De Capua B, Tassi R, et al. Non-functioning posterior communicating arteries of circle of Willis in idiopathic sudden hearing loss. *Lancet* 2000;356:1237–8.

8. Rehm HL, Zhang DS, Brown MC, et al. Vascular defects and sensorineural deafness in a mouse model of Norrie disease. *J Neurosci* 2002;22:4286–92.

9. Schuknecht HF. Myths in neurotology. *Am J Otol* 1992;13:124–6.

10. Haberkamp TJ, Tanyeri HM. Management of idiopathic sudden sensorineural hearing loss. *Am J Otol* 1999;20:587–95.

11. Shaia FT, Sheehy JL. Sudden sensori-neural hearing impairment: a report of 1,220 cases. *Laryngoscope* 1976;86:389–98.

12. Wilkins SA Jr, Mattox DE, Lyles A. Evaluation of a ''shotgun'' regimen for sudden hearing loss. *Otolaryngol Head Neck Surg* 1987;97:474–80.

13. Mattox DE, Simmons FB. Natural history of sudden sensorineural hearing loss. *Ann Otol Rhinol Laryngol* 1977;86:463–80.

14. Patuzzi R, Robertson D. Tuning in the mammalian cochlea. *Physiol Rev* 1988;68:1009–82.

15. Nakashima T, Hattori T, Sone M, et al. Blood flow measurements in the ears of patients receiving cochlear implants. *Ann Otol Rhinol Laryngol* 2002;111:998–1001.

16. Albera R, Ferrero V, Canale A, et al. Cochlear blood flow modifications induced by anaesthetic drugs in middle ear surgery: comparison between sevoflurane and propofol. *Acta Otolaryngol* 2003;123:812–6.

17. Selmani Z, Pyykko I, Ishizaki H, et al. Cochlear blood flow measurement in patients with Meniere's disease and other inner ear disorders. *Acta Otolaryngol Suppl* 2001;545:10–3.

18. Nuttall AL, Hultcrantz E, Larsen HC, et al. Cochlear blood flow increases after systemic hemodilution: comparison of simultaneous laser Doppler flowmetry and radioactive microsphere measurements. *Hear Res* 1988;34:215–23.

19. Miller JM, Goodwin PC, Marks NJ. Inner ear blood flow measured with a laser Doppler system. *Arch Otolaryngol* 1984;110:305–8.

20. Goodwin PC, Miller JM, Dengerink HA, et al. The laser Doppler: a non-invasive measure of cochlear blood flow. *Acta Otolaryngol* 1984;98:403–12.

21. Ren T, Nuttall AL, Miller JM. Relative blood velocity measurement in individual microvessels using the self-mixing effect in a fiber-coupled helium-neon laser. *Microvasc Res* 1995;49:233–45.

22. Mom T, Avan P, Romand R, et al. Monitoring of functional changes after transient ischemia in gerbil cochlea. *Brain Res* 1997;751:20–3.

23. Mom T, Telischi FF, Martin GK, et al. Measuring the cochlear blood flow and distortion-product otoacoustic emissions during reversible cochlear ischemia: a rabbit model. *Hear Res* 1999;133:40–52.

24. Nakashima T, Suzuki T, Iwagaki T, et al. Effects of anterior inferior cerebellar artery occlusion on cochlear blood flow: a comparison between laser-Doppler and microsphere methods. *Hear Res* 2001;162:85–90.

25. Nakashima T, Hattori T, Sone M, et al. Blood flow in the ears of patients receiving cochlear implants. *Ann Otol Rhinol Laryngol* 2004;113:426–30.

26. Ohinata Y, Makimoto K, Kawakami M, et al. Blood flow in common carotid and vertebral arteries in patients with sudden deafness. *Ann Otol Rhinol Laryngol* 1997;106:27–32.

27. Yamasoba T, Kikuchi S, Higo R, et al. Sudden sensorineural hearing loss associated with slow blood flow of the vertebrobasilar system. *Ann Otol Rhinol Laryngol* 1993;102:873–7.

28. Yoneda S, Nukada T, Kimura K, et al. Evaluation of cross-circulation through circle of Willis using an ultrasonic Doppler technique: part II. Comparison between blood flow velocity by ultrasonic Doppler flowmetry and cerebrovascular resistance. *Stroke* 1981;12:484–8.

29. Angelborg C, Axelsson A, Larsen HC. Regional blood flow in the rabbit cochlea. *Arch Otolaryngol* 1984;110:297–300.

30. Axelsson A, Nuttall AL, Miller JM. Observations of cochlear microcirculation using intravital microscopy. *Acta Otolaryngol* 1990;109:263–70.

31. Nuttall AL. Velocity of red blood cell flow in capillaries of the guinea pig cochlea. *Hear Res* 1987;27:121–8.

32. Nuttall AL. Techniques for the observation and measurement of red blood cell velocity in vessels of the guinea pig cochlea. *Hear Res* 1987;27:111–9.

33. Prazma J, Carrasco VN, Garrett CG, et al. Measurement of cochlear blood flow: intravital fluorescence microscopy. *Hear Res* 1989;42:229–36.

34. Ren T, Lin X, Nuttall AL. Polarized-light intravital microscopy for study of cochlear microcirculation. *Microvasc Res* 1993;46:383–93.

35. Kautzky M, Susani M, Franz P, et al. Flexible fiberoptic endoscopy and laser surgery in obliterated cochleas: human temporal bone studies. *Lasers Surg Med* 1996;18:271–7.

36. Baumgartner WD, Franz P, Gstoettner W, et al. Cochlea endoscopy in vivo. *Adv Otorhinolaryngol* 1997;52:62–5.

37. Jung JC, Mehta AD, Aksay E, et al. In vivo mammalian brain imaging using one- and two-photon fluorescence microendoscopy. *J Neurophysiol* 2004;92:3121–33.

38. Jung JC, Schnitzer MJ. Multiphoton endoscopy. *Opt Lett* 2003;28:902–4.

39. Flusberg BA, Jung JC, Cocker ED, et al. In vivo brain imaging using a 3.9 gram two-photon fluorescence microendoscope. *Opt Lett* 2005;30:2272–4.

40. Levene MJ, Dombeck DA, Kasischke KA, et al. In vivo multiphoton microscopy of deep brain tissue. *J Neurophysiol* 2004;91:1908–12.

41. Mehta AD, Jung JC, Flusberg BA, et al. Fiber optic in vivo imaging in the mammalian nervous system. *Curr Opin Neurobiol* 2004;14:617–28.

42. Gomez-Reino C, Perez MV, Bao C. *Gradient-Index Optics*. Berlin: Springer-Verlag, 2002:241.

43. Messerschmidt B, Possner U, Houde-Walter SN. Fabrication tolerances and metrology requirements for ion-exchanged micro-optic lenses: what's good enough? *Appl Opt* 1997;36:8145–52.

44. Diaspro A. *Confocal and two-photon microscopy: foundations, applications, and advances*. New York: Wiley-Liss, 2002:xix, 567.

45. Oldenbourg R, Inoue S, Tiberio R, et al. *Standard Test Targets for High-Resolution Light Microscopy*. Cambridge, UK: Cambridge University Press, 1996:123–38.

46. Asarch R, Abramson M, Litton WB. Surgical anatomy of the guinea pig ear. *Ann Otol Rhinol Laryngol* 1975;84:250–5.

47. Kleinfeld D, Mitra PP, Helmchen F, et al. Fluctuations and stimulus-induced changes in blood flow observed in individual capillaries in layers 2 through 4 of rat neocortex. *Proc Natl Acad Sci U S A* 1998;95:15741–6.

48. Balkany T, Hodges AV, Whitehead M, et al. Cochlear endoscopy with preservation of hearing in guinea pigs. *Otolaryngol Head Neck Surg* 1994;111:439–45.

49. Haapaniemi J, Schrey A, Laurikainen E. The effect of promontorial bone on laser light transmission in measuring capillary blood flow in vivo. *Eur Arch Otorhinolaryngol* 2001;258:209–12.

50. Scheibe F, Haupt H, Berndt H, et al. Laser light transmission and laser Doppler blood flow measurements on the human, rat and guinea pig cochlea. *Eur Arch Otorhinolaryngol* 1990;247:20–3.

51. Miller JM, Bredberg G, Grenman R, et al. Measurement of human cochlear blood flow. *Ann Otol Rhinol Laryngol* 1991;100:44–53.

52. Cooper NP. Harmonic distortion on the basilar membrane in the basal turn of the guinea-pig cochlea. *J Physiol* 1998;509:277–88.

53. Cooper NP, Rhode WS. Nonlinear mechanics at the apex of the guinea-pig cochlea. *Hear Res* 1995;82:225–43.
54. Khanna SM, Hao LF. Nonlinearity in the apical turn of living guinea pig cochlea. *Hear Res* 1999;135:89–104.
55. Khanna SM, Hao LF. Amplification in the apical turn of the cochlea with negative feedback. *Hear Res* 2000;149:55–76.
56. Nuttall AL, Ren T, de Boer E, et al. In vivo micromechanical measurements of the organ of Corti in the basal cochlear turn. *Audiol Neurootol* 2002;7:21–6.
57. Russell IJ, Nilsen KE. The location of the cochlear amplifier: spatial representation of a single tone on the guinea pig basilar membrane. *Proc Natl Acad Sci U S A* 1997;94:2660–4.
58. House HP, Hansen MR, Al Dakhail AA, et al. Stapedectomy versus stapedotomy: comparison of results with long-term follow-up. *Laryngoscope* 2002;112:2046–50.
59. Perkins RC. Laser stapedotomy for otosclerosis. *Laryngoscope* 1980;90:228–40.
60. Vincent R, Oates J, Sperling NM. Stapedotomy for tympanosclerotic stapes fixation: is it safe and efficient? A review of 68 cases. *Otol Neurotol* 2002;23:866–72.
61. Gantz BJ, Turner CW. Combining acoustic and electrical hearing. *Laryngoscope* 2003;113:1726–30.
62. Gstoettner W, Kiefer J, Baumgartner WD, et al. Hearing preservation in cochlear implantation for electric acoustic stimulation. *Acta Otolaryngol* 2004;124:348–52.
63. Gleeson TG, Lacy PD, Bresnihan M, et al. High resolution computed tomography and magnetic resonance imaging in the pre-operative assessment of cochlear implant patients. *J Laryngol Otol* 2003;117:692–5.
64. Federspil PA, Geisthoff UW, Henrich D, et al. Development of the first force-controlled robot for otoneurosurgery. *Laryngoscope* 2003;113:465–71.
65. Federspil PA, Plinkert B, Plinkert PK. Experimental robotic milling in skull-base surgery. *Comput Aided Surg* 2003;8:42–8.
66. Federspil PA, Plinkert PK. Robotic surgery in otorhinolaryngology. *Otolaryngol Pol* 2004;58:237–42.
67. Duan M, Venail F, Spencer N, et al. Treatment of peripheral sensorineural hearing loss: gene therapy. *Gene Ther* 2004;11:S51–6.
68. Garetz SL, Altschuler RA, Schacht J. Attenuation of gentamicin ototoxicity by glutathione in the guinea pig in vivo. *Hear Res* 1994;77:81–7.
69. Lautermann J, McLaren J, Schacht J. Glutathione protection against gentamicin ototoxicity depends on nutritional status. *Hear Res* 1995;86:15–24.